ACS APPLIED MATERIALS & INTERFACES

Research Article

www.acsami.org

Synthesis of Novel Acceptor Molecules of Mono- and Multiadduct Fullerene Derivatives for Improving Photovoltaic Performance

Chao Liu,[†,‡] Liang Xu,[†,‡] Dan Chi,[†,§] Yongjun Li,[†] Huibiao Liu,*[,†] and Jizheng Wang[†]

[†]Beijing National Laboratory for Molecular Sciences (BNLMS), CAS Key Laboratory of Organic Solids, Institute of Chemistry, Chinese Academy of Sciences, Beijing 100190, People's Republic of China

[‡]University of Chinese Academy of Sciences, Beijing 100049, People's Republic of China

[§]Key Laboratory of Semiconductor Materials Science, Institute of Semiconductors, Chinese Academy of Sciences, Beijing, 100083, People's Republic of China

Supporting Information

ABSTRACT: We have successfully synthesized and separated a series of *tert*-butyl 4-C_{61}-benzoate (***t*-BCB**) organofullerenes, including monoadduct, diadduct, and triadduct compounds, and investigated their photophysics, electrochemistry, thermal properties, and high-performance liquid chromatography analysis. The photovoltaic devices were fabricated based on monoadduct, diadduct, and triadduct products, and the devices based on them exhibited power conversion efficiencies of 2.43%, 0.48%, and 1.68%, respectively. This was the first time to study the dependent relationship on the device performance and the different isomer numbers.

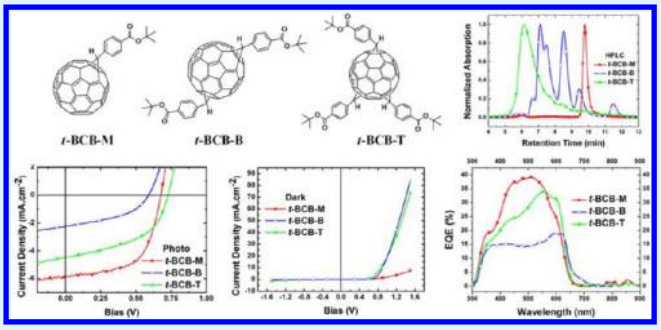

KEYWORDS: *bulk heterojunction, fullerene, photovoltaic property, multiadduct*

1. INTRODUCTION

Fullerene derivatives are extensively used in organic photovoltaics (OPVs) because of their high electron affinity and high mobility[1−7] and remarkable properties on photoinduced electron transfer.[8−11] In recent decades, [6,6]-phenyl-C_{61}-butyric acid methyl ester ($PC_{61}BM$) is widely studied, and scientists have reported much work on utilizing $PC_{61}BM$ and new improved fullerene materials.[2,12−22] A mixture of Bis- and Tri-$PC_{61}BM$ was first applied in bulk-heterojunction (BHJ) OPVs by Padinger et al., and they found that the multiadduct PCBM can provide a high-quality film and the lowest short-circuit current density (J_{SC}), 5.6 times smaller than that of Mono-PCBM.[23] Brabec et al. found that the open-circuit voltage (V_{OC}) was related to the lowest unoccupied molecular orbital (LUMO) energy level of the acceptor (A) and highest occupied molecular orbital (HOMO) energy level of the donor (D).[24] Afterward, Blom et al. purified Bis-PCBM and prepared the BHJ OPVs with poly(3-hexylthiophene)(P3HT), contributing to a PCE of 4.5%, V_{OC} of 0.73 V, a fill factor (FF) of 68%, and J_{SC} of 9.14 mA·cm^{-2} in 2008.[22] Since then, Laird et al. applied indene−fullerene diadduct first in BHJ OPVs, which was a D−A reaction production of 56π electrons.[19]

Because fullerene is a three-dimensional (3D) ball,[25−28] there are lots of reactive sites on the ball with little steric hindrance,[29−33] contributing multiadduct fullerene compounds with dozens of isomers.[34] Blom et al. measured the photovoltaic performance, mobility, and isomer numbers of mono-, di-, and triadduct fullerene analogues using BHJ OPVs, a space-charge-limited current (SCLC) method, and high-performance liquid chromatography (HPLC), respectively; they found that the diadduct could increase V_{OC}, while J_{SC} would decrease because of the bigger isomer numbers and lower mobility of multiadduct fullerene.[20] Our previous work reported that even diadduct fullerene derivatives may have bigger isomer numbers, lower mobility, and lower performance than that of monoadduct.[35] This is due to the fact that bigger isomer numbers lead to lower mobility. The multiadducts are of great importance both in applications as acceptor materials in organic solar cell and in understanding the properties of multiadducts on the interface and surface.[36,37] However, there have been no reports in the fabrication of photovoltaic devices based on triadduct (54π) or tetraadduct (52π) fullerene materials with higher performance. Here, we report studies on the synthesis and photovoltaic devices of the ***t*-BCB** series (Figure 1) of fullerene materials of monoaddition (***t*-BCB-M**), diaddition (***t*-BCB-B**), and triaddition (***t*-BCB-T**).

2. EXPERIMENTAL SECTION

Materials and Equipment. All solvents were purified and freshly distilled prior to use according to literature procedures and a purification handbook. Commercially available materials were used as received. Synthesis, experimental, and characterization conditions and detailed data are given in the Supporting Information. C_{60}, 99.9%,

Received: November 26, 2012
Accepted: December 31, 2012
Published: December 31, 2012

   dx.doi.org/10.1021/am3028475 | *ACS Appl. Mater. Interfaces* 2013, 5, 1061−1069

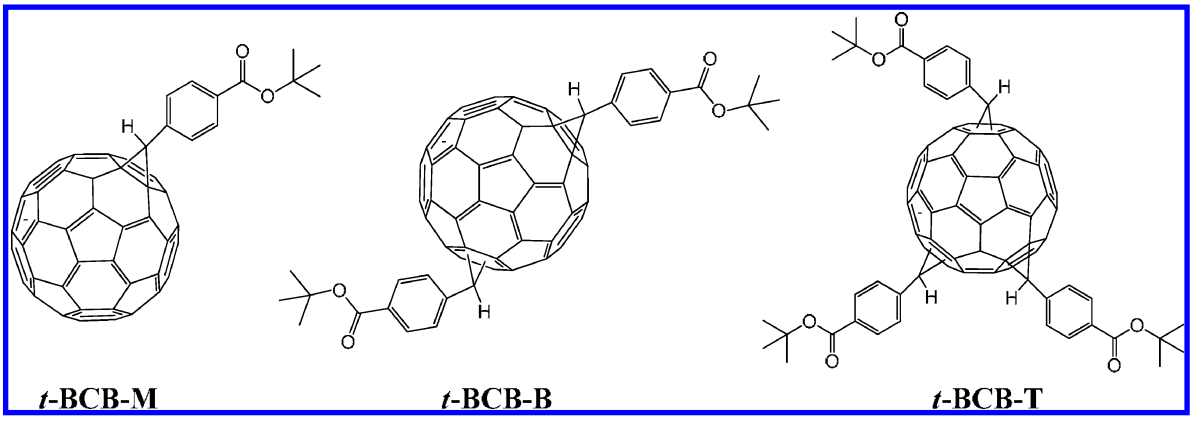

Figure 1. Structures of *t*-**BCB** fullerene derivatives.

was provided by the Henan Yongxin Company, People's Republic of China; ferrocene (A.R.) was bought from China National Medicines Corp. Ltd. and then extracted by hexane; *o*-dichlorobenzene for synthesis and cyclic voltammetry (CV) was of HPLC-grade and was supplied by Ouhe Chemicals Corp., Beijing, People's Republic of China, and for device fabrication was supplied by Aldrich with 98+% purity of Extra Dry and acroseal; poly(3-hexylthiophene-2,5-diyl) was bought from Aldrich. Poly(ethylenedioxythiophene):poly-(styrenesulfonic acid) (PEDOT:PSS) was CLEVIOS A1 4083; $TBAPF_6$ (A.R.) was bought from Alfa, then recrystallized in ethanol two times, and dried in vacuo at 80 °C.

Synthesis. The detailed synthesis of the precursors is reported in the Supporting Information. The [6,6]-phenyl-C_{61} derivatives were synthesized according to the method developed by Hummelen et al.[38] *tert*-Butyl 4-(diazomethyl)benzoate (330 mg, 3 equiv) from the previous step was dissolved in dry pyridine (15 mL) under nitrogen and stirred at room temperature for 15−30 min, and then a solution of fullerene (360 mg, 1 equiv) in dry 1,2-dichlorobenzene (*o*-DCB; 50 mL) was added. The mixture was stirred at 80−120 °C for 12−24 h, and then the solvent was removed in vacuo. The crude product was chromatographed on silica gel (200−300 mesh) by 0−50% ethyl acetate in toluene as the eluent. Each portion of different adducts was collected and purified by chromatography on silica gel (300−400 mesh) again, then resolved in phenyl chloride (PhCl), and refluxed for 72 h to ensure most of the [5,6] open-shell isomers changed to [6,6] closed-shell methanofullerenes (product refluxed in *o*-DCB will partly decompose, while the rating change was slow; thus, 72 h was necessary, as confirmed by Buckyprep HPLC analysis). After removal of PhCl in vacuo, the product was purified by chromatography on silica gel (300−400 mesh) to remove some decomposition compounds. Then the product was dissolved in a little dichloro-methane, precipitated with methanol, centrifuged, and decanted. The remaining pellet was washed three times with methanol in a supersonic bath to remove small molecule impurities; moreover, *n*-hexane and ethyl ether were used to treat materials with previous precipitation and washing procedures in sequence to remove silica and impurities in the solvent. Finally, all materials were dried in vacuo at 45 °C for 24−48 h, resulting in the purest [6,6]methanofullerene derivatives that we can produce. The multiadduct fullerenes were analyzed by HPLC on an analytical Cosmosil Buckyprep column [4.6 mm (i.d.) × 250 mm], using toluene as the eluent at a flow rate of 0.6 mL/min, to give some information about the minimum number of isomers.

***t*-BCB-M**. Yield: 20%. ^{1}H NMR (600 MHz, $CDCl_3$): δ 8.19 (d, J = 6.8 Hz, 2H), 8.05 (d, J = 6.7 Hz, 2H), 5.43 (s, 1H), 1.64 (s, 9H). IR (KBr, cm^{-1}): ν 2974 (w), 2924 (m), 2854 (w), 1712 (s), 1611 (w), 1511 (w), 1456 (m), 1383 (m), 1289 (m), 1254 (w), 1161 (s), 1110 (s), 802 (w), 740 (w), 575 (w), 524 (m), 466 (m). MALDI-TOF CCA. Found: m/z 910.3 (M^-). Calcd ($C_{72}H_{14}O_2$): m/z 910.10. Described ref 38.

***t*-BCB-B**. Yield: 40%. ^{1}H NMR (600 MHz, $CDCl_3$): δ 8.35−7.76 (m, 4H), 5.56−4.88 (m, 1H), 1.87−1.46 (m, 9H). IR (KBr, cm^{-1}): ν2974 (w), 2927 (w), 1715 (s), 1611 (m), 1500 (w), 1456 (m), 1367 (m), 1291 (s), 1256 (w), 1164 (s), 1117 (s), 1019 (m), 849 (w), 767 (w), 704 (w), 524 (m), 419 (w). MALDI-TOF CCA. Found: m/z 1100.5 (M^-). Calcd ($C_{84}H_{28}O_4$): m/z 1100.20.

***t*-BCB-T**. Yield: 30%. ^{1}H NMR (600 MHz, $CDCl_3$): δ 8.45−7.66 (m, 4H), 5.57−3.46 (m, 1H), 1.84−1.42 (m, 9H). IR (KBr, cm^{-1}): ν 3418 (w), 2974 (m), 2927 (m), 1715 (s), 1610 (m), 1507 (m), 1454 (m), 1394 (w), 1291 (s), 1254 (w), 1165 (s), 1114 (s), 1019 (m), 847 (m), 763 (m), 704 (m), 522 (m). MALDI-TOF CCA. Found: m/z 1290.4 (M^-). Calcd ($C_{96}H_{42}O_6$): m/z 1291.30.

Measurement. ^{1}H and ^{13}C NMR spectra were measured on Bruker DMX300 and Avance 400 or 600 spectrometers and calibrated using signals from trimethylsilane (TMS) and reported downfield from TMS. Matrix-assisted laser desorption ionization time-of-flight mass spectra (MALDI-TOF-MS) were measured on a Bruker Biflex III MALDI-TOF spectrometer and gave M^-, consistent with the calculated mass of all synthesized C_{60} derivatives. The Fourier transform infrared spectra were measured on a Bruker Tensor-27 spectrometer and showed absorption features at ca. 526 cm^{-1} indicative the [60]fullerene core. Thermogravimetric/differential thermal analysis (TGA/DTA) was measured on a Shimadzu DTG-60 analyzer. Differential scanning calorimetry (DSC) measurement was performed on a PerkinElmer Diamond differential scanning calorimeter (N536-0022). The thickness of the film was tested by a profilometer on a Tencor ALFA-Step 500 or an Ambios Technology XP-2. Atomic force microscopy (AFM) was measured on a SII SPA400 microscope, in tapping mode (DFM). HPLC was tested on a JAI LC-9104 chromatograph in cooperation with a Cosmosil Buckyprep 20 mm (ID) × 250 mm column for preparation, and also a Waters 660 chromatograph in cooperation with a Cosmosil Buckyprep Waters 4.6 mm (ID) × 250 mm column for analysis. CV was measured on a Chi660d.Optical microscope (OM) on an Olympus BX51. UV−vis spectra were tested on a Jasco V-570 spectrometer.

The space charge is defined when excess charge was used as a continuum charge distributed in the internal region of a semi-conductor. The SCLC method was used to test hole and electron mobility in the direction perpendicular to the electrodes, which is a typical method for testing the charge-carrier mobility for OPVs.[39,40] Electron-only devices with the structure Al/active layer/Al were fabricated, and their current−voltage (J−V) characteristics in dark have been measured. According to eq 1

$$J = \frac{9}{8}\varepsilon_r\varepsilon_0\mu_e\frac{V^2}{L^3} \quad (1)$$

where J is the current density, V is the applied voltage, ε_r and ε_0 are the relative dielectric constant of the organic layer (ε_r = 3) and the permittivity of free space (8.854×10^{-14} F/cm), respectively, μ_e is the electron mobility, and L is the thickness of the organic layer.

Hole-only devices with the structure indium/tin oxide (ITO)/PEDOT:PSS/active layer/Au were also fabricated according to eq 2

$$J \cong \frac{9}{8}\varepsilon_r\varepsilon_0\mu_h V^2 \exp(0.89\sqrt{V/E_0 L})L^3 \quad (2)$$

where $V = V_{appl} - V_{bi}$, V_{appl} is the applied voltage, V_{bi} is the compensation voltage, around 0.2 V, μ_h is hole mobility, and E_0 is a constant in room temperature.

Fabrication and Characterization of OPVs. The device structure used in this study was a classic sandwich structure with ITO/PEDOT as a hole-collecting electrode and Al as an electron-collecting electrode, i.e., glass/ITO/PEDOT:PSS/P3HT:fullerene/Ca/Al (Figure 2). ITO (150 nm thickness) glasses were cleaned by

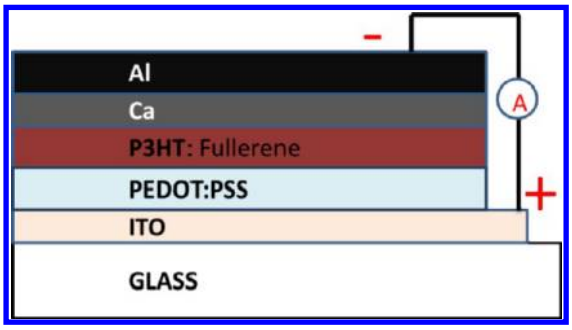

Figure 2. Schematic layout of an organic BHJ solar cell.

supersonic treatment in acetone, water, acetone, and isopropyl alcohol for at least 10 min, respectively, and then by O_2 plasma treatment for 6 min with 300 W, which was used as the anode, and a thin layer of PEDOT:PSS was incorporated between the ITO and active layer to reduce device leakage, which was around 30-nm-thick spin-coated at 4000 rpm for 60 s and baked at 140 °C for 10 min to dryness. Methanofullerenes and P3HT in different weight ratios were mixed and then dissolved in an *o*-DCB solution, both usually 17 mg/mL. The solution was spin-coated onto the top of PEDOT:PSS at different rates for different times to optimize the device performance. In the structure of the devices, the active layer had a thickness of around 90−200 nm. The time for solvent annealing (SA) was around 30 min, and then prethermal annealing (PTA) was performed at 110 °C for 30 min or 150 °C for 10 min in a glovebox and then cooled in N_2 in a glovebox. At last, a Ca layer of 30 nm and an Al layer of 80 nm were thermally deposited on the active layer in vacuo. The deposition rates, usually 0.05−0.10 nm/s, and the thicknesses of the evaporation layers were monitored by a thickness/rate meter (FTM-V). The crossing area between the cathode and anode defined the sensing area. The device area was 0.036 cm^2 or 0.04 cm^2 calibrated by an OM. All of the fabrication steps were carried out in a nitrogen glovebox with H_2O < 0.1 ppm and O_2 < 0.1 ppm. The *J*−*V* measurement of the devices was conducted on a computer-controlled Keithley 236 source measure unit. Device characterization was done in a glovebox under simulated AM 1.5G irradiation (100 mW/cm^2) using a Newport xenon-lamp-based solar simulator. The external quantum efficiency (EQE) measurements of the OPVs were performed using a Stanford Research Systems model SR830 DSP lock-in amplifier coupled with a WDG3 monochromator and a 500 W xenon lamp. The light intensity at each wavelength was calibrated with a standard single-crystal silicon photovoltaic cell. We tried various weight ratios of the polymer and fullerene, film thicknesses, additives (1-bromothiophene), temperatures, and time of thermal annealing to optimize the devices to their best performance.

3. RESULTS AND DISCUSSION

UV−Vis. Absorption, especially in the visible region, is a very important property for the photovoltaic materials.[10,28,41,42] The visible spectra of the fullerene derivatives in a ca. 10^{-5} M toluene solution are shown in Figure 3 in calibration to concentration, and the peak data are listed in Table 1. All of these fullerene derivatives have weak absorption in ca. 700 nm,

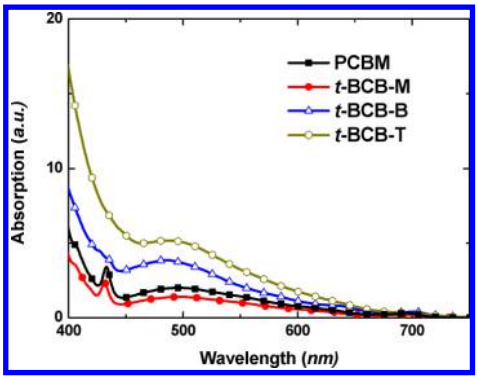

Figure 3. UV−vis absorption spectra of fullerene solution, calibrated by concentration.

Table 1. UV−Vis Absorbance Peak Data

fullerene	400−450 (nm)	450−600 (nm)	>600 (nm)
PCBM	433	496	697
***t*-BCB-M**	431	495	697
***t*-BCB-B**		486	704
***t*-BCB-T**		498	

confirming that the three fullerenes were [6,6]-methanofullerene as opposed to [5,6] and [6,6] mixtures.[43] The absorption of monoadduct ***t*-BCB-M** was weaker than that of PCBM, but the band structures were similar, while the triadduct and diadduct's absorptions were much stronger than those of ***t*-BCB-M** and PCBM, indicating that the multiadduct has changed the electron structures of the C_{60} cage enormously, with the absorption relation of ***t*-BCB-T** > ***t*-BCB-B** > PCBM > ***t*-BCB-M**.

Thermal Analysis. Samples were kept at 100 °C in vacuo for 24 h before thermal analysis. TGA/DTA was measured to understand the thermal stability of the fullerene derivatives, as shown in Figure 4 and Table 2, which indicate that all fullerene derivatives have a thermal decomposition temperature higher than 200 °C (onset temperature), i.e., 223, 228, and 209 °C respectively for ***t*-BCB-M**, ***t*-BCB-B**, and ***t*-BCB-T**, which ensured the OPV devices to be safe for thermal annealing treatment. DSC showed no crystallization (T_c) or glass transitions (T_g) between 20 and 200 °C, which suggested that the ***t*-BCB** series was amorphous materials.[2]

Electrochemistry. The electrochemical property is one of the most important properties of fullerenes.[44−46] The value of the difference between the LUMO of the acceptor and the HOMO of the donor is related to V_{OC};[24,47−50] therefore, the LUMO energy levels of the fullerene derivatives are crucial for their application in OPVs as acceptors, which can be measured by CV and differential pulse voltammetry (DPV). We measured all of the reduction potentials of the three fullerene derivatives, shown in Table 3 and Figure 5. The LUMO energy levels were estimated from the onset value of their first reduction potential (E^1_{red}) according to eq 3.

$$\text{LUMO} = -\text{e}(E^1_{red} + 4.80) \quad (3)$$

The further addition of the three organofullerenes, the smaller E^1_{red}, and the higher LUMO of the fullerene derivatives, due to saturation of the double bonds of the fullerene cage,[20] are consistent with the recent multiadduct fullerene reported.[2,20,22] Thus, the E^1_{red} values of the ***t*-BCB** series decreased successively from ***t*-BCB-M** to ***t*-BCB-T**, and their

dx.doi.org/10.1021/am3028475 | ACS Appl. Mater. Interfaces 2013, 5, 1061−1069

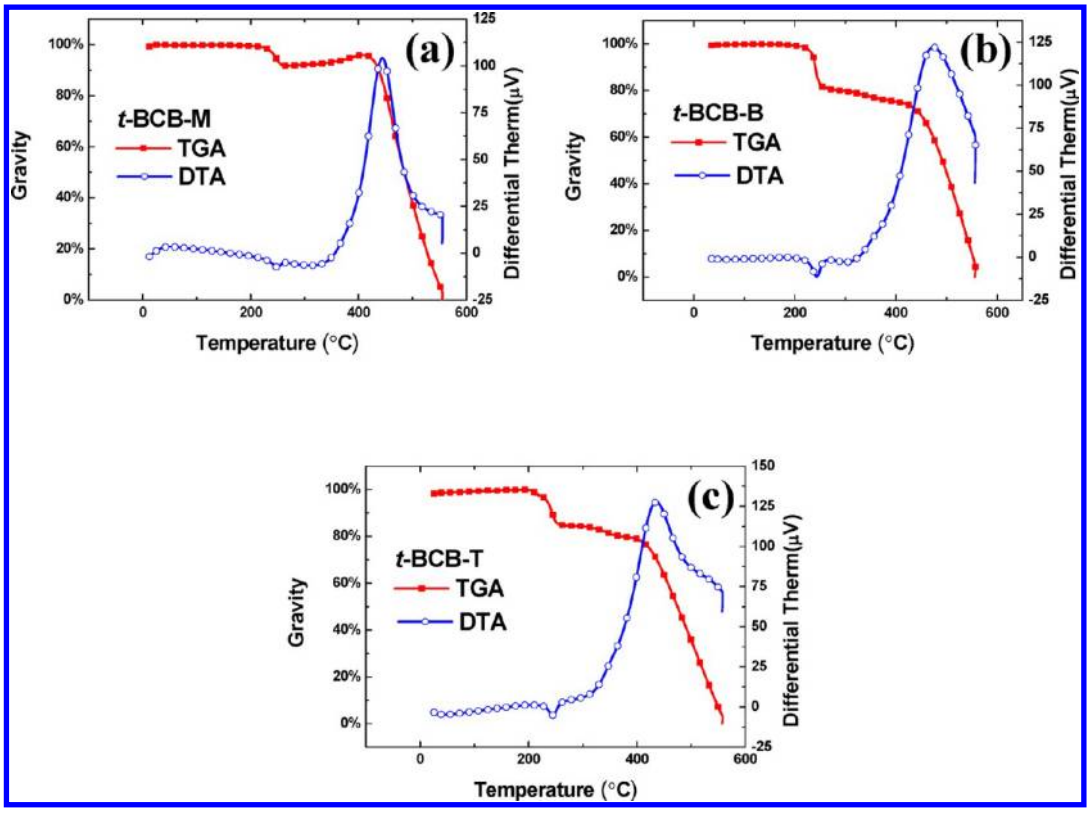

Figure 4. TGA/DTA of a ***t*-BCB** series of fullerenes: (a) ***t*-BCB-M**; (b) ***t*-BCB-B**; (c) ***t*-BCB-T**.

Table 2. Decomposition Temperatures of the *t*-BCB Series

fullerene	T_d^{onset} (°C)	weight loss (%)
***t*-BCB-M**	223	6.2
***t*-BCB-B**	228	16.2
***t*-BCB-T**	209	12.2

Table 3. Electrochemistry Properties of Fullerene Derivatives[a]

fullerene	E^1_{red} (V)	LUMO (eV)	Δ (eV)
C_{60}	−1.02	−3.78	−0.07
PCBM	−1.09	−3.71	0.00
***t*-BCB-M**	−1.06	−3.74	−0.03
***t*-BCB-B**	−1.15	−3.65	0.06
***t*-BCB-T**	−1.18	−3.62	0.09

[a] E^1_{red} are onset values in V vs Fc/Fc^+ (internal standard) by CV with 10^{-4}–10^{-3} M *o*-DCB solution; tetrabutylammonium hexafluorophosphate ($TBAPF_6$, 0.1 M) was used as the supporting electrolyte, platinum wire as the counter electrode, silver wire as the reference electrode, glassy carbon as the working electrode, and ferrocene as the internal standard; the scan rate was 50 mV/s; the room temperature was ca. 25 °C. Δ was compared to PCBM's LUMO level.

LUMO energy levels increased successively. The LUMO energy level of ***t*-BCB-M** was 0.03 eV lower than that of PCBM because of the electron-withdrawing effect of the carbonyl group on the phenyl ring. ***t*-BCB-M** was electro-reversible as testified by the symmetric peaks, equal i_{pa} and i_{pc}, small ΔE_p value of the redox couples in the CV and also sharp and clean DPV peaks, while ***t*-BCB-B** and ***t*-BCB-T** were electro-quasi-reversible because the peak-to-peak separation, ΔE_p ($\Delta E_p = E_p^c - E_p^a$, where E_p^a is the anodic peak potential and E_p^c is the catholic peak potential), was much bigger than 60 mV, as shown in Table 4, indicating that their ability to accept an electron and then transfer the electron was weaker than that of their monoadduct analogue, resulting in lower J_{SC}.[51]

Photovoltaics. The solubility of fullerene ***t*-BCB-M** was approximately 10 mg/mL lower than others in an *o*-DCB solution, while the devices based on it by a solution of 15 mg/mL led to an incontinuous "film" with islands of 50 μm diameter observed by an OM (Figure 6), whose performance was short circuit. When we reduced the concentration to 10 and 5 mg/mL, the films were continuous with the thickness about 50 nm with PCE of 2.43%. Its series resistance (R_S) was really low, about 0.7 Ω·cm^2, compared to that of common devices, which might be a result of the high conductivity of ***t*-BCB-M** (Figures 7 and 8 and Table 5). Notably, there were three abnormal and interesting phenomena in the performance.

(i) Usually, the LUMO energy levels of fullerene materials as the acceptor and shunt resistance (R_{SH}) of devices are both directly positively correlated with V_{OC};[52] i.e., V_{OC} would increase with an increase of the LUMO energy level or an increase of R_{SH}. Although the LUMO energy level of ***t*-BCB-M** is 0.03 eV lower than that of PCBM and R_{SH} of ***t*-BCB-M** was 3 times smaller than that of PCBM, which should perform a much lower V_{OC} than that of PCBM with both negative factors; oppositely, the V_{OC} of ***t*-BCB-M** is 0.03−0.05 V higher than that of PCBM, which was confirmed in hundreds of devices. (ii) The LUMO energy levels of the three materials are stepwise increased with the number of additions. The V_{OC} value of ***t*-BCB-T** is 0.05 V higher than that of ***t*-BCB-M**, which is consistent with the relation of their LUMO energy levels, albeit the V_{OC} value of ***t*-BPC-B** was oppositely lower than that of the others; meanwhile the J_{SC} and FF values of ***t*-BCB-B** was the lowest among the three, which suggested that ***t*-BCB-T** had more terrible contact with the electrode than the others,

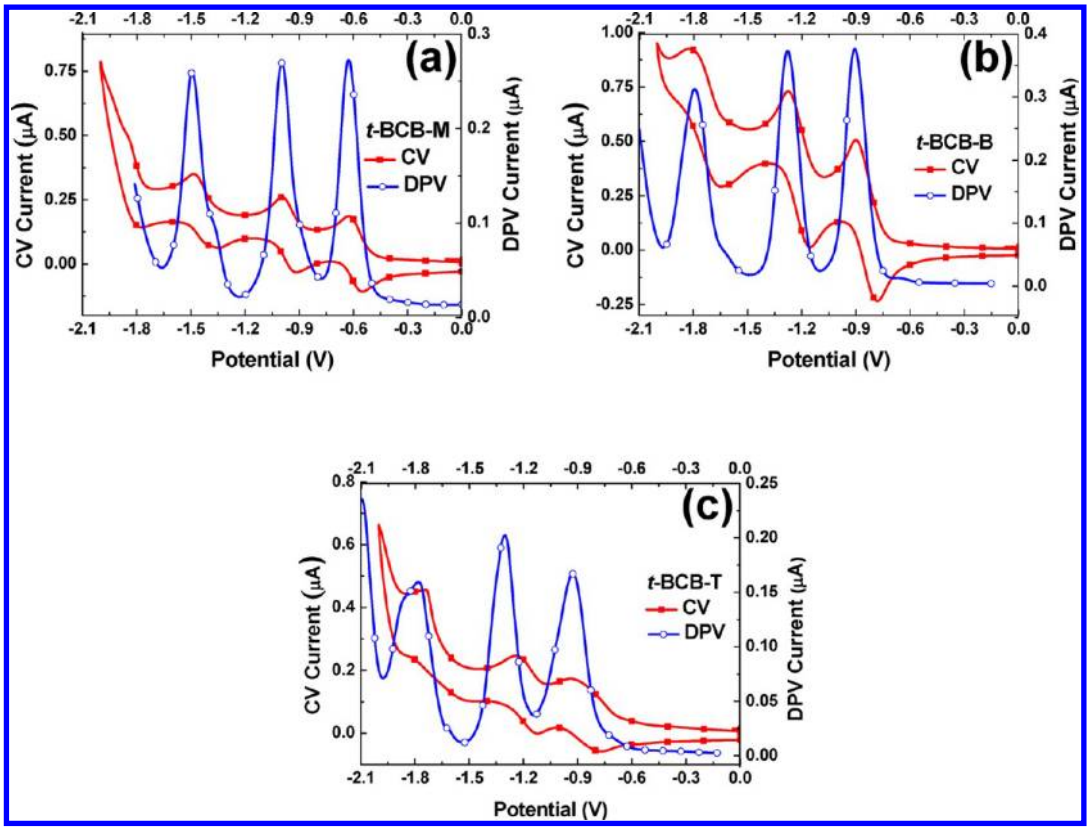

Figure 5. CV and DPV figures of ***t*-BCB-M** (a), ***t*-BCB-B** (b), and ***t*-BCB-T** (c). The CV figures were compared to a silver wire electrode, and DPV figures were calibrated to the first reduction potential of the CV.

Table 4. ΔE_p of Each Reduction Potential of Three Fullerenes

fullerene	reduction potential	E_{red}^{lowest} (V vs Fc/Fc$^+$)	ΔE_p (mV)
***t*-BCB-M**	E^1	−1.06	75
***t*-BCB-M**	E^2	−1.40	75
***t*-BCB-M**	E^3	−1.83	138
***t*-BCB-B**	E^1	−1.15	121
***t*-BCB-B**	E^2	−1.48	127
***t*-BCB-B**	E^3	−1.94	178
***t*-BCB-T**	E^1	−1.19	160
***t*-BCB-T**	E^2	−1.56	120
***t*-BCB-T**	E^3	−2.08	281

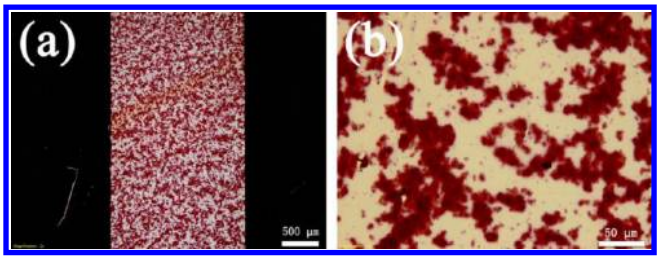

Figure 6. OM pictures of incontinuous films of ***t*-BCB-M** based on OPVs fabricated by a solution of 15 mg/mL.

confirmed by the highest R_S. The bigger isomer number and lower mobility might contribute to the lowest J_{SC} value, as suggested by the literature[2,20] and the mobility experiment below. (iii) Generally, higher addition fullerene derivatives contribute to more isomers; however, there are also exceptions caused by steric hindrance or special reaction procedures; e.g., Nakamura et al. found that a single isomer pentaadduct can be generated by an organic copper reagent.[53,54] The disorder of verified isomers directly lead to the lower mobility and lower J_{SC},[2,20] and a possible explanation for this decrease was that the macroscopic mobility was an average of all orientations, and isomers increased the disorder strongly also destroyed crystallization of the polymer, resulting in lower absorption and lower mobility of the active layer film,[55,56] although higher adducts may have higher V_{OC}. To our surprise, The performance of ***t*-BCB-T** was much better than that of ***t*-BCB-B**, with both J_{SC} and FF higher than those of the diadduct. We speculated that the abnormal more excellent performance of ***t*-BPB-T** than ***t*-BCB-B** was related to a fewer isomers of the triadduct rather than the diadduct. HPLC, ^{1}H NMR, SCLC, and UV−vis confirmed our theory.

HPLC figures (Figure 9a) of the three organofullerenes did not give the information of the exact isomer number by a Buckyprep HPLC column, even tested by the mixed-solvent eluents of toluene and isopropyl alcohol with different ratios;[20] however, the information of the minimal isomer number can be shown, which clearly indicated that the isomer number of ***t*-BCB-B** was much bigger than that of ***t*-BCB-T**. In light of the spin−spin-coupling splitting, the ^{1}H NMR peaks of the isomers were not exact for the isomer numbers, and also the signal-to-noise ratios were low in the case of ***t*-BCB-B** and ***t*-BCB-T**, no matter how many samples were tested in the NMR tubes. Therefore, the featured proton signal of ArC(C_{60})*H* (Figure 9b) around 5.43 ppm of ^{1}H NMR was not sufficient evidence to confirm the relation between ***t*-BCB-B** and ***t*-BCB-T**, which only showed that there were at least 10 isomers in both the diadduct and triadduct.

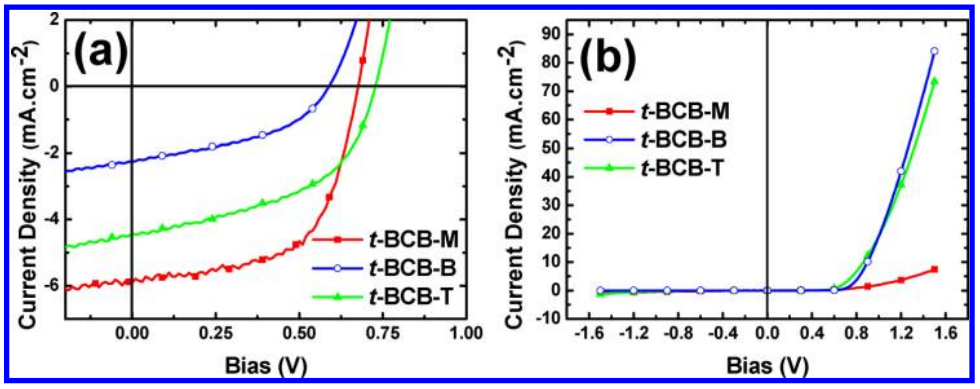

Figure 7. *J*–*V* curves of P3HT/***t*-BCB** devices: (a) photocurrent; (b) dark current.

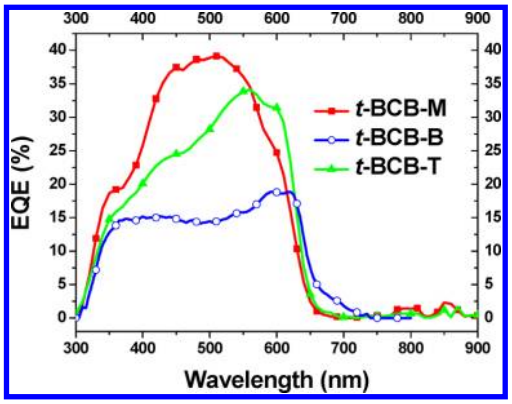

Figure 8. EQEs of devices based on ***t*-BCB** materials.

Table 5. Photovoltaic Performance Indices of P3HT/*t*-BCB Devices

fullerene	PCE (%)	V_{OC} (V)	J_{SC} (mA/cm^2)	FF (%)	R_S (Ω·cm^2)	R_{SH} (Ω·cm^2)
PCBM	3.8	0.63	8.9	64	4.5	2566
***t*-BCB-M**	2.43	0.68	5.9	61	0.7	783
***t*-BCB-B**	0.41	0.59	2.3	44	6.1	616
***t*-BCB-T**	1.68	0.73	4.4	56	5.5	551

Now that it was known that the mobility of fullerenes was directly related to the isomer number and photovoltaic performance, we measured the mobility of ***t*-BCB-B** and ***t*-BCB-T**. Their film was mixed with P3HT by the SCLC method (Table 6) and prepared using optimized conditions, fabricating the photovoltaic devices. The results showed that the electron

Table 6. Mobility of *t*-BCB and P3HT: *t*-BCB Film Tested by SCLC

active layer	μ_e (cm^2/V·s)	μ_h (cm^2/V·s)	μ_h/μ_e
***t*-BCB-B**	3.7×10^{-8}	3.2×10^{-5}	8.7×10^{2}
***t*-BCB-T**	8.3×10^{-6}	7.2×10^{-5}	8.6
P3HT:***t*-BCB-B**	5.0×10^{-8}	4.2×10^{-4}	8.4×10^{3}
P3HT:***t*-BCB-T**	1.2×10^{-4}	7.6×10^{-4}	6.5
P3HT:PCBM[57]	2.3×10^{-4}	3.1×10^{-4}	1.4

mobilities (μ_e) of the two were remarkably different; i.e., μ_e of ***t*-BCB-T** was 100 times higher than that of ***t*-BCB-B**, and μ_e of its BHJ film was 10000 times higher than that of ***t*-BCB-B**. The difference of the hole mobility (μ_h) was not as obvious as that of μ_e; i.e., μ_h of ***t*-BCB-T** was 2.2 times higher than that of ***t*-BCB-B**, and μ_h of its BHJ film was 1.8 times higher than that of ***t*-BCB-B**. The mobility test directly proved the abnormal photovoltaic performances of ***t*-BCB-B** and ***t*-BCB-T**. In summary, attributed to the strong steric hindrance of the *tert*-butyl group of the adduct, the isomer number of the triadduct was smaller than that of the diadduct, which was reasonable and gave new insight on how to design higher adduct fullerene materials with higher LUMO and V_{OC}.

The value of the ratio of the hole-to-electron mobilities (μ_h/μ_e) of the film is crucial to understanding the photovoltaic process of BHJ OPVs. We calculated and compared μ_h/μ_e values summed in Table 6. P3HT:PCBM (according to ref 57), ***t*-BCB-T**, and P3HT:***t*-BCB-T** showed relatively well-balanced ratios, whereas ***t*-BCB-B** and P3HT:***t*-BCB-B** showed unbalanced ratios (8.7×10^2 and 8.4×10^3, respectively) because of their lower μ_e values. Balanced electron–hole transport is detrimental to increases in FF.[58,59] As shown by the ratio of

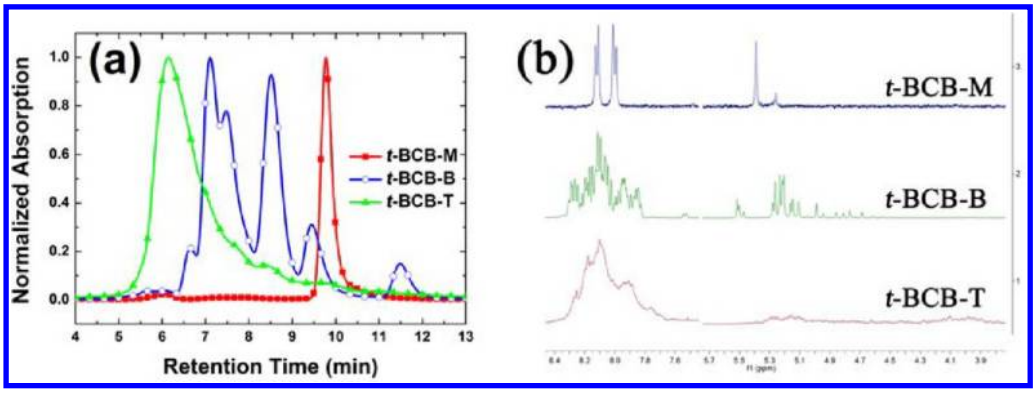

Figure 9. HPLC figures (a) and ^{1}H NMR spectra (b) of ***t*-BCB**.

P3HT:*t*-**BCB-B**, charge accumulation can occur in the active layer, and the photocurrent is space-charge-limited, when the charge transport in the device is strongly unbalanced. In this case, the photocurrent is governed by a square-root dependence on the bias, and a high FF cannot be reached.[57−59] However, when the carrier transport is well-balanced, such as for P3HT:PCBM and P3HT:*t*-**BCB-T**, the photocurrent is not limited by space-charge effects and relatively high FF can be achieved. Herein, the unbalanced μ_h/μ_e value is another factor contributing to the lower J_{SC} and FF of *t*-**BCB-B** rather than *t*-**BCB-T**.

Morphology. The morphology of the devices was studied by AFM, which can reveal the surface nanostructures,[60,61] parts of the 3D nanostructure of the BHJ film.[62−64] OM results (Figure 6) showed that there were lots of fullerene crystals precipitating in *t*-**BCB-M**-based devices, around 3−10 μm, while **B**- and **C**-based devices seemed smooth with little fullerene precipitated. AFM showed (Figures 10−12 and S10 and S11 in the Supporting Information) that the scale of the phase separation of *t*-**BCB-M**-based devices was 50−100 nm, which was bigger than that of PCBM at 10−30 nm, while for *t*-**BCB-B**-based devices, the scale of phase separation was 30−100 nm. The largest scale of phase separation was that of *t*-**BCB-T**-based devices, about 1−2 μm, where the fullerene seemed to be lying on the surface of the polymers, and the larger scale of phase separation hindered charge transfer then decreased the mobility and J_{SC},[65,66] which directly confirmed why *t*-**BCB-T** showed terrible OPV performance, i.e., because of bad miscibility.

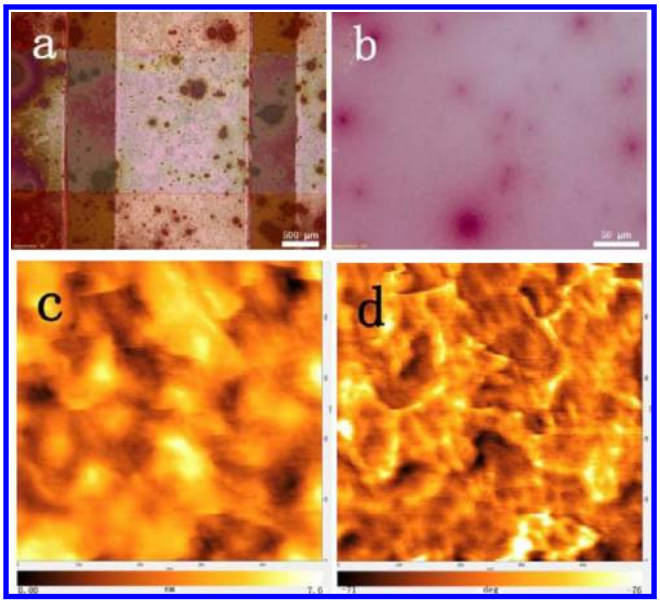

Figure 10. Morphology images of *t*-**BCB-M**-based devices: (a) and (b), OM pictures; (c), AFM hight image; (d), AFM phase image, 500 nm × 500 nm.

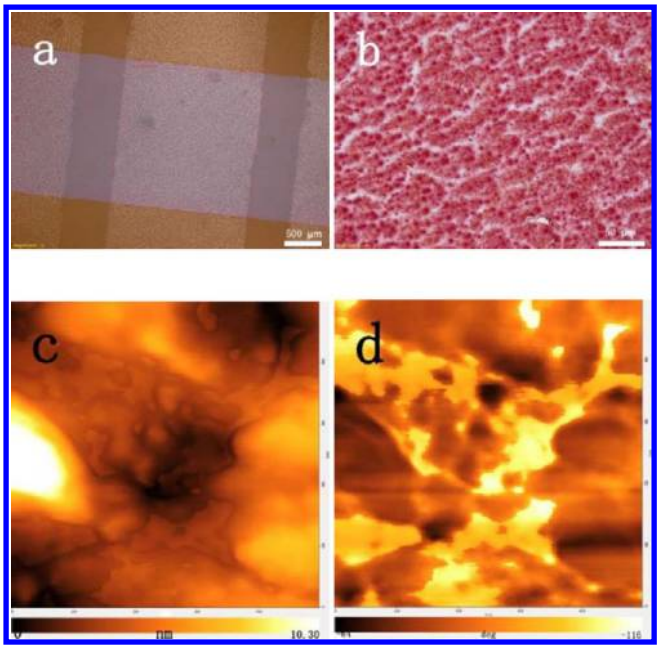

Figure 11. Morphology images of *t*-**BCB-B**-based devices: (a) and (b), OM pictures; (c), AFM hight image; (d), AFM phase image, 500 nm × 500 nm.

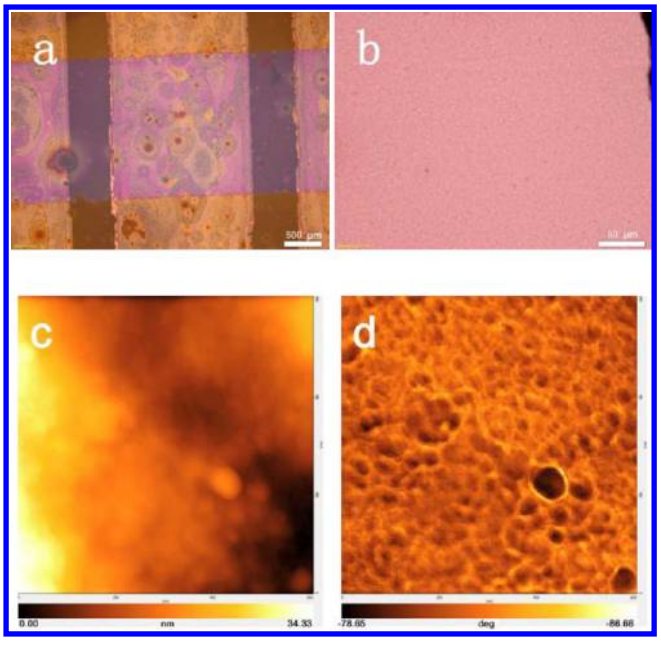

Figure 12. Morphology images of *t*-**BCB-T**-based devices: (a) and (b), OM pictures; (c), AFM hight image; (d), AFM phase image, 500 nm × 500 nm.

4. CONCLUSIONS

We have successfully synthesized three new fullerene derivatives including mono-, di-, and triadduct compounds, and the photophysical properties of these fullerene derivatives were investigated. The monoadduct's device exhibits a power conversion efficiency of 1.67% near PCBM's 2.43% in the conditions of SA and pre-thermal annealing. Our results also indicate that the semireversible redox electrochemistry properties and larger phase separation of multiadducts can lead to lower mobility and result in the lower photovoltaic performance of multiadduct materials. While smaller number of isomers of triadduct than that of diadduct because of the hindrance of tert butyl group, contributed to higher mobility of triadduct than that of diadduct, meanwhile the more balanced hole-to-electron mobility ratio of triadduct than that of bisadduct led to the previous higher FF. This work provides new evidence and a route to design fullerene materials with high mobility, V_{OC}, J_{SC}, molar absorption, and device performance. The fundamental

dx.doi.org/10.1021/am3028475 | ACS Appl. Mater. Interfaces 2013, 5, 1061−1069

studies operated here will definitely be helpful to understanding the work mechanism of mono- and multiadduct solar cells and imply that such organofullerene materials are promise building blocks for the development of high-performance solar power conversion systems.

■ ASSOCIATED CONTENT

Supporting Information

Description of the synthesis, NMR, IR, MS, equipment, and reagents. This material is available free of charge via the Internet at http://pubs.acs.org.

■ AUTHOR INFORMATION

Corresponding Author

*E-mail: liuhb@iccas.ac.cn.

Notes

The authors declare no competing financial interest.

■ ACKNOWLEDGMENTS

This work was supported by the National Nature Science Foundation of China (Grants 21031006, 90922007, 21021091, and 21290190) and the National Basic Research 973 Program of China (Grant 2011CB932302).

■ REFERENCES

(1) Yu, G.; Gao, J.; Hummelen, J. C.; Wudl, F.; Heeger, A. J. *Science* **1995**, *270*, 1789−1791.
(2) Liu, C.; Xiao, S.; Shu, X.; Li, Y.; Xu, L.; Liu, T.; Yu, Y.; Zhang, L.; Liu, H.; Li, Y. *ACS Appl. Mater. Interfaces* **2012**, *4*, 1065−1071.
(3) Wang, G. W.; Zhu, B. *Chem. Commun.* **2009**, 1769−1771.
(4) Zheng, H.; Li, Y.; Liu, H.; Yin, X.; Li, Y. *Chem. Soc. Rev.* **2011**, *40*, 4506−4524.
(5) Xiao, S.; Li, Y.; Li, Y.; Zhuang, J.; Wang, N.; Liu, H.; Ning, B.; Liu, Y.; Lu, F.; Fan, L.; Yang, C.; Li, Y.; Zhu, D. *J. Phys. Chem. B* **2004**, *108*, 16677−16685.
(6) Wang, N.; Li, Y. J.; He, X. R.; Gan, H. Y.; Li, Y. L.; Huang, C. S.; Xu, X. H.; Xiao, J. C.; Wang, S.; Liu, H. B.; Zhu, D. B. *Tetrahedron* **2006**, *62*, 1216−1222.
(7) Liu, H.; Xu, J.; Li, Y.; Li, Y. *Acc. Chem. Res.* **2010**, *43*, 1496−1508.
(8) Huang, C.; Lu, F.; Li, Y.; Gan, H.; Jiu, T.; Xiao, J.; Xu, X.; Cui, S.; Liu, H.; Zhu, D. *J. Nanosci. Nanotechnol.* **2007**, *7*, 1472−1478.
(9) Huang, C.; Wang, N.; Li, Y.; Li, C.; Li, J.; Liu, H.; Zhu, D. *Macromolecules* **2006**, *39*, 5319−5325.
(10) Jiang, L.; Chang, Q.; Ouyang, Q.; Liu, H.; Wang, Y.; Zhang, X.; Song, Y.; Li, Y. *Chem. Phys.* **2006**, *324*, 556−562.
(11) Zhu, D.; Li, Y.; Wang, S.; Shi, Z.; Du, C.; Xiao, S.; Fang, H.; Zhou, Y. *Synth. Met.* **2003**, *133*−*134*, 679−683.
(12) Matsuo, Y.; Sato, Y.; Niinomi, T.; Soga, I.; Tanaka, H.; Nakamura, E. *J. Am. Chem. Soc.* **2009**, *131*, 16048−16050.
(13) Li, C.-Z.; Matsuo, Y.; Niinomi, T.; Sato, Y.; Nakamura, E. *Chem. Commun.* **2010**, *46*, 8582−8584.
(14) Cheng, Y.-J.; Liao, M.-H.; Chang, C.-Y.; Kao, W.-S.; Wu, C.-E.; Hsu, C.-S. *Chem. Mater.* **2011**, *23*, 4056−4062.
(15) Zhang, C.; Chen, S.; Xiao, Z.; Zuo, Q.; Ding, L. *Org. Lett.* **2012**, *14*, 1508−1511.
(16) Meng, X.; Zhang, W.; Tan, Z. a.; Li, Y.; Ma, Y.; Wang, T.; Jiang, L.; Shu, C.; Wang, C. *Adv. Funct. Mater.* **2012**, *22*, 2187−2193.
(17) Meng, X.; Zhang, W.; Tan, Z. a.; Du, C.; Li, C.; Bo, Z.; Li, Y.; Yang, X.; Zhen, M.; Jiang, F.; Zheng, J.; Wang, T.; Jiang, L.; Shu, C.; Wang, C. *Chem. Commun.* **2012**, *48*, 425−427.
(18) Mikroyannidis, J. A.; Tsagkournos, D. V.; Sharma, S. S.; Sharma, G. D. *J. Phys. Chem. C* **2011**, *115*, 7806−7816.
(19) Laird, D. W.; Richter, H.; Vejins, V.; Scott, L.; A., L. T.; Stegamat, R.; Malika, D. WO2009086210A2, 2009.
(20) Lenes, M.; Shelton, S. W.; Sieval, A. B.; Kronholm, D. F.; Hummelen, J. C.; Blom, P. W. M. *Adv. Funct. Mater.* **2009**, *19*, 3002−3007.
(21) Ross, R. B.; Cardona, C. M.; Guldi, D. M.; Sankaranarayanan, S. G.; Reese, M. O.; Kopidakis, N.; Peet, J.; Walker, B.; Bazan, G. C.; Van Keuren, E.; Holloway, B. C.; Drees, M. *Nat. Mater.* **2009**, *8*, 208−212.
(22) Lenes, M.; Wetzelaer, G. J. A. H.; Kooistra, F. B.; Veenstra, S. C.; Hummelen, J. C.; Blom, P. W. M. *Adv. Mater.* **2008**, *20*, 2116−2119.
(23) Padinger, F.; Brabec, C. J.; Fromherz, T.; Hummelen, J. C.; Sariciftci, N. S. *Opto-Electron. Rev.* **2000**, *8*, 280−283.
(24) Brabec, C. J.; Cravino, A.; Meissner, D.; Sariciftci, N. S.; Fromherz, T.; Rispens, M. T.; Sanchez, L.; Hummelen, J. C. *Adv. Funct. Mater.* **2001**, *11*, 374−380.
(25) Lu, F. S.; Li, Y. L.; Liu, H. B.; Zhuang, J. P.; Gan, L. B.; Zhu, D. B. *Synth. Met.* **2005**, *153*, 317−320.
(26) Luo, H.; Liu, H.; Li, Y.; Shi, Z.; Fang, H.; Li, H.; Xiao, S.; Xiao, S.; Zhu, D. *Synth. Met.* **2003**, *135*−*136*, 845−846.
(27) Fang, H.; Xiao, S.; Li, Y.; Xiao, S.; Li, H.; Liu, H.; Shi, Z.; Zhu, D. *Synth. Met.* **2003**, *135*−*136*, 837−838.
(28) Xiao, S. Q.; Li, Y. J.; Li, Y. L.; Liu, H. B.; Li, H. M.; Zhuang, J. P.; Liu, Y.; Lu, F. S.; Zhang, D. Q.; Zhu, D. B. *Tetrahedron Lett.* **2004**, *45*, 3975−3978.
(29) Li, Y. J.; Gan, Z. H.; Wang, N.; He, X. R.; Li, Y. L.; Wang, S.; Liu, H. B.; Araki, Y.; Ito, O.; Zhu, D. B. *Tetrahedron* **2006**, *62*, 4285−4293.
(30) Xiao, S.; El-Khouly, M. E.; Li, Y.; Gan, Z.; Liu, H.; Jiang, L.; Araki, Y.; Ito, O.; Zhu, D. *J. Phys. Chem. B* **2005**, *109*, 3658−3667.
(31) Liu, H. B.; Zhao, Q.; Li, Y. L.; Liu, Y.; Lu, F. S.; Zhuang, J. P.; Wang, S.; Jiang, L.; Zhu, D. B.; Yu, D. P.; Chi, L. F. *J. Am. Chem. Soc.* **2005**, *127*, 1120−1121.
(32) Lu, F. S.; Xiao, S. Q.; Li, Y. L.; Liu, H. B.; Li, H. M.; Zhuang, J. P.; Liu, Y.; Wang, N.; He, X. R.; Li, X. F.; Gan, L. B.; Zhu, D. B. *Macromolecules* **2004**, *37*, 7444−7450.
(33) Zhang, Q.; Jia, Z.; Liu, S.; Zhang, G.; Xiao, Z.; Yang, D.; Gan, L.; Wang, Z.; Li, Y. *Org. Lett.* **2009**, *11*, 2772−2774.
(34) Zhang, G.; Liu, Y.; Liang, D.; Gan, L.; Li, Y. *Angew. Chem., Int. Ed.* **2010**, *49*, 5293−5295.
(35) Liu, C.; Li, Y.; Li, C.; Li, W.; Zhou, C.; Liu, H.; Bo, Z.; Li, Y. *J. Phys. Chem. C* **2009**, *113*, 21970−21975.
(36) Fang, H.; Du, C.; Qu, S.; Li, Y.; Song, Y.; Li, H.; Liu, H.; Zhu, D. *Chem. Phys. Lett.* **2002**, *364*, 290−296.
(37) Li, Y.; Liu, Y.; Wang, N.; Li, Y.; Liu, H.; Lu, F.; Zhuang, J.; Zhu, D. *Carbon* **2005**, *43*, 1968−1975.
(38) Hummelen, J. C.; Knight, B. W.; LePeq, F.; Wudl, F.; Yao, J.; Wilkins, C. L. *J. Org. Chem.* **1995**, *60*, 532−538.
(39) Rose, A. *Phys. Rev.* **1955**, *97*, 1538−1544.
(40) Murgatroyd, P. N. *J. Phys. D: Appl. Phys.* **1970**, *3*, 151.
(41) Barszcz, B.; Graja, A.; Liu, C.; Li, Y. L. *Synth. Met.* **2010**, *160*, 2351−2354.
(42) Li, H.; Li, Y.; Zhai, J.; Cui, G.; Liu, H.; Xiao, S.; Liu, Y.; Lu, F.; Jiang, L.; Zhu, D. *Chem.—Eur. J.* **2003**, *9*, 6031−6038.
(43) Janssen, R. A. J.; Hummelen, J. C.; Wudl, F. *J. Am. Chem. Soc.* **1995**, *117*, 544−545.
(44) Gan, H. Y.; Liu, H. B.; Li, Y. L.; Gan, L. B.; Jiang, L.; Jiu, T. G.; Wang, N.; He, X. R.; Zhu, D. B. *Carbon* **2005**, *43*, 205−208.
(45) Xiao, S.; Li, Y.; Fang, H.; Li, H.; Liu, H.; Shi, Z.; Jiang, L.; Zhu, D. *Org. Lett.* **2002**, *4*, 3063−6.
(46) Shi, Z. Q.; Li, Y. L.; Gong, H. F.; Liu, M. H.; Xiao, S. X.; Liu, H. B.; Li, H. M.; Xiao, S. Q.; Zhu, D. B. *Org. Lett.* **2002**, *4*, 1179−1182.
(47) He, Y. J.; Li, Y. F. *Phys. Chem. Chem. Phys.* **2011**, *13*, 1970−1983.
(48) Scharber, M. C.; Wuhlbacher, D.; Koppe, M.; Denk, P.; Waldauf, C.; Heeger, A. J.; Brabec, C. L. *Adv. Mater.* **2006**, *18*, 789−794.
(49) Fang, H.; Wang, S.; Xiao, S.; Yang, J.; Li, Y.; Shi, Z.; Li, H.; Liu, H.; Xiao, S.; Zhu, D. *Chem. Mater.* **2003**, *15*, 1593−1597.
(50) Fang, H.; Wang, S.; Xiao, S.; Li, Y.; Shi, Z.; Du, C.; Zhou, Y.; Zhu, D. *Macromol. Chem. Phys.* **2002**, *203*, 1931−1935.

(51) Echegoyen, L.; Echegoyen, L. E. *Acc. Chem. Res.* **1998**, *31*, 593−601.
(52) Gu, J.; Zhong, Z.; He, X.; Sun, F.; Chen, S. *J. South-Cent. Univ. Natl., Nat. Sci. Ed.* **2009**, *28*, 57−61.
(53) Sawamura, M.; Iikura, H.; Nakamura, E. *J. Am. Chem. Soc.* **1996**, *118*, 12850−12851.
(54) Matsuo, Y.; Nakamura, E. *Chem. Rev.* **2008**, *108*, 3016−3028.
(55) Yun, M. H.; Kim, G.-H.; Yang, C.; Kim, J. Y. *J. Mater. Chem.* **2010**, *20*, 7710−7714.
(56) Liu, Y.; Xiao, S. Q.; Li, H. M.; Li, Y. L.; Liu, H. B.; Lu, F. S.; Zhuang, J. P.; Zhu, D. B. *J. Phys. Chem. B* **2004**, *108*, 6256−6260.
(57) Kang, H.; Cho, C.-H.; Cho, H.-H.; Kang, T. E.; Kim, H. J.; Kim, K.-H.; Yoon, S. C.; Kim, B. J. *ACS Appl. Mater. Interfaces* **2011**, *4*, 110−116.
(58) Mihailetchi, V. D.; Xie, H. X.; de Boer, B.; Koster, L. J. A.; Blom, P. W. M. *Adv. Funct. Mater.* **2006**, *16*, 699−708.
(59) Blom, P. W. M.; Mihailetchi, V. D.; Koster, L. J. A.; Markov, D. E. *Adv. Mater.* **2007**, *19*, 1551−1566.
(60) Cui, S.; Liu, H.; Gan, L.; Li, Y.; Zhu, D. *Adv. Mater.* **2008**, *20*, 2918−2925.
(61) Xiao, J.; Liu, Y.; Li, Y.; Ye, J.; Li, Y.; Xu, X.; Li, X.; Liu, H.; Huang, C.; Cui, S.; Zhu, D. *Carbon* **2006**, *44*, 2785−2792.
(62) Zhuang, J.; Zhou, W.; Li, X.; Li, Y.; Wang, N.; He, X.; Liu, H.; Li, Y.; Jiang, L.; Huang, C.; Cui, S.; Wang, S.; Zhu, D. *Tetrahedron* **2005**, *61*, 8686−8693.
(63) Liu, H. B.; Li, Y. L.; Jiang, L.; Luo, H. Y.; Xiao, S. Q.; Fang, H. J.; Li, H. M.; Zhu, D. B.; Yu, D. P.; Xu, J.; Xiang, B. *J. Am. Chem. Soc.* **2002**, *124*, 13370−13371.
(64) Wang, N.; Lu, F. S.; Huang, C. S.; Li, Y. L.; Yuan, M. J.; Liu, X. F.; Liu, H. B.; Gan, L. B.; Jiang, L.; Zhu, D. B. *J. Polym. Sci., Part A: Polym. Chem.* **2006**, *44*, 5863−5874.
(65) Jo, J.; Na, S. I.; Kim, S. S.; Lee, T. W.; Chung, Y.; Kang, S. J.; Vak, D.; Kim, D. Y. *Adv. Funct. Mater.* **2009**, *19*, 2398−2406.
(66) Muller-Buschbaum, P.; Ruderer, M. A. *Soft Matter* **2011**, *7*, 5482−5493.